Research article

Design and testing of a hybrid electromagnetic damping device for automotive applications

Amer Alhams [a], Abdulhafiz Qazak [a], Yousif Badri [b], Sadok Sassi [a,*], Jamil Renno [a], Abdelmonaam Sassi [c]

[a] Department of Mechanical and Industrial Engineering, Qatar University, Qatar
[b] Department of Mechanical Engineering, University of Auckland, New Zealand
[c] Department of Civil Engineering, Windsor University, Canada

ARTICLE INFO

ABSTRACT

This study proposes a new design concept for combining a viscous fluid damper (VFD) with an eddy current damper (ECD). Three main concepts were thoroughly discussed: the magnetic system, the conductive material, and the housing. In particular, the excitation circuit and magnetic field were applied from the exterior of the main chamber of the VFD to minimize the intrusive risks introduced into the damper when trying to connect an internal magnetic system to an external power source.

Experimental investigations on a test rig developed for this purpose were carried out in this work. The design aimed to generate eddy currents in an oscillating cylinder made of copper placed around an existing real-world car damper and secured to its moving rod. When exposed to an electromagnetic field, the newly designed system rapidly generated an extra level of damping in addition to the initial damping effect provided by the viscous mechanism. The obtained results showed that applying an electric current of only 1A increased the amplitude of the drag force by 12 % for an electrode with a thickness of 1.5 mm. A magnetic saturation phenomenon resisted any extra increase in the current. Making the metal conductor thicker is expected to increase the volume of the conductor in which the currents are flowing and, consequently, increase the damping effect.

1. Introduction

Automobiles have become more than just a mode of transportation; they are now an integral part of our lives. In the US, for example, each American travels for an average of 46 min per day [1]. In automobiles, different sources of vibrations might compromise the driver's comfort and the vehicle's stability. They could be internal (induced by the rotating parts and especially the engine) or external to the automobile's structure (arising from the interaction of the tires with irregularities or imperfections in the road). Therefore, automobile suspension systems have been carefully designed as isolation systems between the vehicle's chassis and road-induced disturbances. Furthermore, the suspension system enhances the vehicle's stability on the road by minimizing fluctuations in the tire's normal force. The damper, also called a shock absorber, is the essential element of all suspension systems. Connecting a dissipative element (a damper) in parallel with an elastic element significantly reduces the effects of a sudden bump by damping and

smoothening the shock. There are three types of suspension dampers commonly used to address a vehicle's instabilities: passive, semi-active (also known as hybrid or semi-passive), and active dampers. Various hybrid damping solutions have been suggested, such as those utilizing electro-rheological fluids [2,3] and magneto-rheological fluids [4,5,6]. The eddy current damper (ECD) is a third design for semi-passive suspension systems.

When diamagnetic materials (also referred to as conductors) come into contact with a field that is continuously changing, it results in the generation of what is known as eddy currents (EC) within the material (as shown in Fig. 1) [7]. These eddy currents produce a field that opposes the field that caused them, causing a force that counteracts the motion between the material and the magnetic field. These effects are achieved through Lenz's law. According to this law, a current induced by a changing magnetic field will always act in opposition to the change in flux [8]. Because of its effectiveness, the EC effect has been widely used in various industrial applications such as nondestructive testing, braking

systems, and generating electrical energy.

As automobile manufacturers strive to provide increased safety and comfort for passengers, using EC-damping devices in automobiles has become increasingly popular [9]. The use of the EC technique in automotive damping devices has been widely studied in the past few years, and many publications related to this topic can be found in the literature [10]. Several studies have shown that ECs can effectively lower the vibration level of automotive damping devices. However, an EC damper (ECD) must be connected to an AC source for maximum efficiency. Indeed, connecting it to a DC source creates a powerful but very short pulse of change in the magnetic field. One of the most significant drawbacks of the ECD is its low damping efficiency, as it produces weaker resistive forces relative to the weight and size of the magnet and conductor [11]. Therefore, different studies have focused on improving damping efficiency by optimizing the design's structure, the magnets' configuration, and the type of diamagnetic material [11,12].

Several authors have recently studied the possibility of using ECDs in automotive suspension systems using analytical modeling, finite element simulation, and experimental testing. In most investigations, the model was based on permanent magnets (PMs) (Fig. 2). In [13], the authors designed a passive ECD with a set of PMs and used a thick aluminum pipe as a conductor. Furthermore, several designs applied the Halbach Array Orientation to optimize the magnets' configuration, resulting in a higher flux density and more significant current induction [14,15]. In [16], the authors used rare earth PMs (NdFeB) in their tuned mass damper (TMD) and concluded that, because of ECDs' wide range of operating frequency (from 0.1 Hz to 10 Hz), it did not induce extra stiffness at any operating frequency. Hence, it could be used to tune TMDs and increase the efficiency of their damping performance.

An ECD can also be implemented to store energy. For example, in a theoretical investigation where an ECD model could use impact loads to store energy [17], the efficiency reached 2.33 %. In a more recent investigation [18], the authors measured the damping coefficient in a stationary-conductor ECD with a perpendicular motion, resulting in a 6 % error compared with the 3D finite element (FE) analysis results. Furthermore, the influence of vibrations on the structure of a solar panel was investigated using ECDs [19], and the authors discovered that the magnetic flux reduced exponentially when the air gap separating the magnet and the rotating conductor increased. In a comprehensive study [20], the authors modeled, designed, and tested a vehicle with an ECD,

in which the FE model validated their predictions and the experimental data, but their damper involved only PMs.

Furthermore, some methodologies for predicting and calculating the induced damping force and stiffness of different magnets were proposed in [21] and used to evaluate the efficiency of passive ECD models. Recently, improvements in the efficiency of ECD were achieved [22] by presenting and modeling a dual-sided hybrid ECD that enhanced the damping effect in a system with a linear motion. Later in the same year, another design was proposed [23] for a regenerative ECD considering PMs on B-class vehicle dampers.

So far, ECDs have been used directly as dampers for dissipating energy and reducing vibrations or as a damping element within tuned mass dampers (TMDs) [12]. Nevertheless, according to the best of our knowledge, there has been no attempt to combine an ECD with a conventional automotive hydraulic damper in an industrial application. Therefore, we designed a new ECD for suppressing vibrations in automobiles. The ECD was added to a conventional viscous fluid damper (VFD) to create a hybrid device where the damping value can be changed when needed, thus providing a semi-active control strategy. The damping performance of the newly developed ECDs for use in automobiles was verified through experiments and simulations. The basic concept used in constructing the hybrid damping device was to combine an ECD system with a standard VFD, already preinstalled on a car suspension. Combining both damping devices in parallel rather than depending on a single one resulted in a fail-safe system that could vary damping forces within the entire system. If a fault within the electromagnetic device occurred, the VFD could still suppress and dampen the vibrations as a regular passive damper.

This article has been organized as follows. Section 2 presents the design of the hybrid ECD. The computational approach and analysis of the magnetic performance are outlined in Section 3. The experimental testing setup is explained in Section 4, whereas Section 5 presents and discusses the results. Section 6 presents the conclusion.

2. Design of the ECD damper

To optimize the overall effectiveness, several significant factors must be addressed in the design of the EC damping device. These include the dimensions of the different constituents of the system, the type of magnetic material, the conductive material's permeability, the air gap
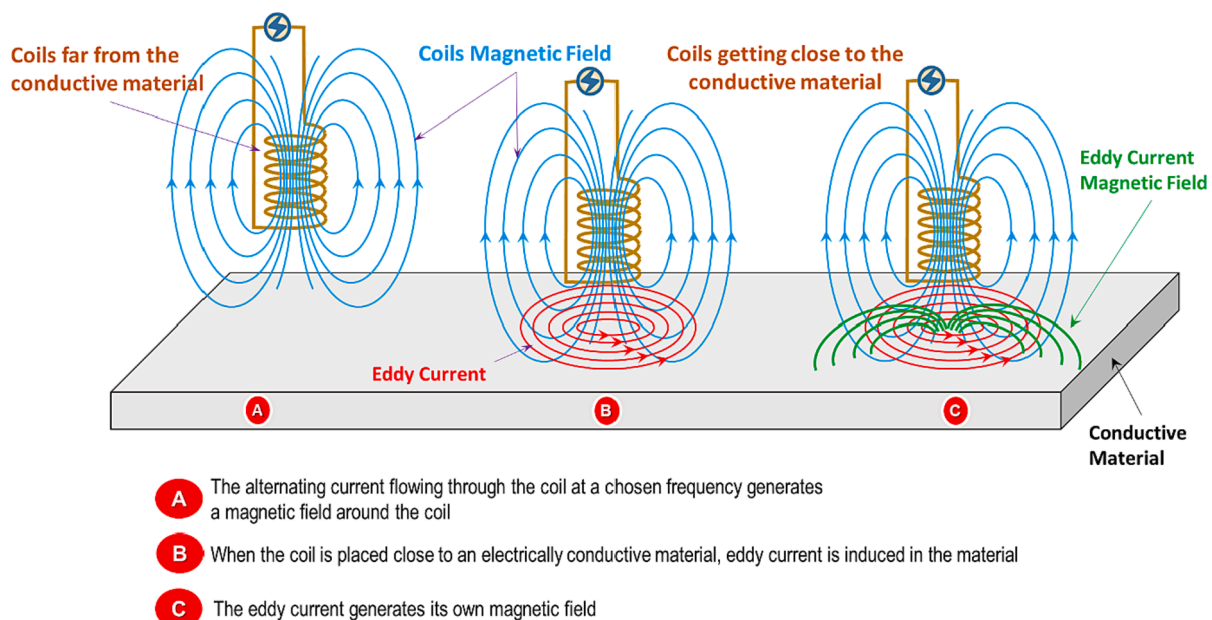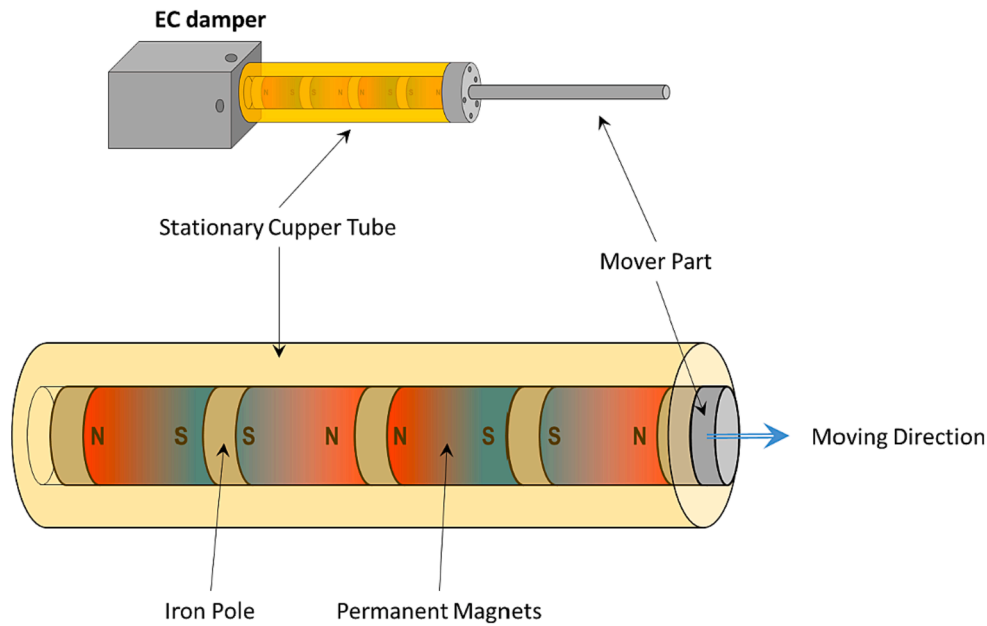

Fig. 1. Generation of ECs.

Fig. 2. Classical design of a magnetic (EC) damper based on PMs.

between the fixed and moving parts, and the thickness of the metal conductor.

2.1. Effects of the air gap

The air gap within a magnetic circuit is generally a dual-purpose element. Sometimes, it could be fundamental for ensuring the device works well, while in other cases, it should be minimized. The presence of an air gap helps reduce the impact of saturation in the core, preventing the circuit from losing its energy storage capabilities. It can also be used to improve the efficiency of a magnetic circuit and protect the core from damage caused by excessive magnetic flux density. However, an air gap may be an unwanted phenomenon. It forms an isolation layer that significantly compromises the effectiveness of ECs. As the air gap increases, some magnetic flux can escape through it and will move sideways. This dispersion of the flux lines reduces the stored energy generated by the magnetic field. A study of disk braking systems in electric motorcycles found that the air gap affected the braking performance by influencing the behavior of ECs [24]. More recently, a study focusing on storing energy in magnetic devices with an air gap [25] proved that the stored energy decreased with increased air gap length. In the present investigation, for the sake of efficiency and in line with previous analyses, the gap between the moving conductor pipe and the stationary cores was minimized to 1.5 mm to maximize the induced current's potential while offering the moving parts the needed safe distance that avoids any risk of touching each other.

2.2. Effects of the thickness of the metal conductor

The magnitude of the EC can be influenced by various factors, such as the metal thickness, its conductivity, and its permeability. For instance, its thickness can affect how much magnetic energy is able to penetrate the metal and how much surface area is available for the flow of current. It is true that the density of an EC is highest at the surface of the conductor but reduces exponentially as the depth increases; this is known as the skin effect [26]. It is true that the density of an EC is highest at the surface of the conductor but reduces exponentially as the depth increases; this is known as the skin effect [26]. However, a thicker conductor allows for a greater flow of EC since the conductor's increased cross-sectional area provides more surface area for the current to flow

without generating as much heat. Hence, thicker conductors will have lower resistance and lower EC losses than thinner conductors. Nevertheless, thicker conductors may have higher material costs and be more challenging to work within certain applications. Therefore, it is essential to consider the conductor's electrical and mechanical properties when selecting a suitable thickness for a particular application. Because of the constraints related to the materials available on the local market, the most affordable and suitable copper pipe for the suggested design was 76 mm in diameter with a wall thickness of 1.5 mm. Although thicker walls would be more suitable for better efficiency, the available thickness should be enough to prove the concept.

2.3. Selection of the magnet and conductive material

There are two types of magnets that can be used in an ECD: electromagnets and permanent magnets. Permanent magnets are made of natural magnetic minerals like cobalt, iron, and nickel and can generate a magnetic field without the use of external power sources. They are more durable and unaffected by external factors such as temperature and electrical fields. Neodymium magnets are a type of permanent magnet that has stronger remanence, coercivity, and energy compared to other types of magnets. However, they are fragile and can break easily if not handled carefully. They are also more expensive than ceramic magnets and must be coated to prevent corrosion. Electromagnets, on the other hand, are created by wrapping a conductor around a magnetic core and producing a magnetic field when an electric current is passed through the wire. They can be easily switched on and off, and their strength can be adjusted by changing the current intensity flowing through the coil.

In summary, Electromagnets are more versatile than permanent magnets, as they can be used in industrial applications, like ours, where the magnet strength needs to be adjusted. Furthermore, electromagnets can provide a greater magnetic flux with an appropriate arrangement of coils, wire thickness, and number of turns in the same area.

Moreover, to control the damping properties better, an electromagnet should preferably create the magnetic field, as the magnetic field's intensity is proportional to the excitation current feeding the coils. The main idea in the actual design was to leave the primary damping mechanism based on a conventional viscous damper and to use the ECD only when needed. According to the literature, none of the

previous work on ECDs has considered using electromagnets in the ECDs of vehicle suspension systems, making the novelty of this work evident. Therefore, electromagnets were used in the novel ECD design.

2.4. Design specifications

Before producing any ECD device for automotive purposes, the first challenge is to decide whether to incorporate a dual damping mechanism (such as hydraulic and EC, magneto-rheological and EC, electro-rheological and EC, etc.) or to rely solely on an ECD system. The current research combined the traditional hydraulic damping mechanism with an ECD system for optimal efficiency and safety. This approach ensured that the overall damping system did not break down in case of a malfunction in the magnetizing system since the original hydraulic damper would continue to function as it would in traditional circumstances.

Typically, combining a VFD and ECD side by side, similar to the traditional parallel damper scheme (Fig. 3), is a straightforward way to integrate both components. However, this configuration creates an unstable arrangement because the two branches have unequal stiffness, resulting in an unequal distribution of forces. Therefore, to achieve symmetry in the overall system and to balance the difference in stiffness between the two branches, the ECD could be positioned between two identical VFDs. Alternatively, to solve the same problem more efficiently and cost-effectively, both dampers can be placed on the same axis, with one damper encapsulated within the other. Compared with the first design, this second approach is more practical because it saves space, which is critical in automotive suspensions. Encapsulating the ECD inside the hydraulic damper allows both damping effects to be present in one component, reducing the size and weight of the overall system. The traditional hydraulic damper can provide smooth and predictable damping, while the ECD can provide an additional rapid damping response in urgent situations. Combining these damping effects in one compact device and reducing the overall size can improve the system's performance and prevent unwanted phenomena such as structural resonance.

However, there are a few disadvantages to this approach. Encapsulating the ECD within the hydraulic damper increases the system's complexity because it requires a long drilling operation to ensure electricity supply to the coil from an external energy source. In the most common type of mono-coil piston assembly (Fig. 4), the magnetic flux is adjusted by the current flowing through a coil embedded within the piston that is fixed to the rod. To make such an action possible, it would be necessary to make very deep holes along the rod to introduce the wires supplying electricity. If the ratio of depth to diameter (L/d) is > 10, this type of drilling is known as deep-hole drilling. This is a highly complex manufacturing process. During deep-hole drilling, it is challenging to achieve tight control of the diameter, keep the hole straight, and remove chips without causing damage to the surface and avoiding damage to the drilling tool. Making such holes disrupts the smooth operation of the damper and frequently allows the fluid in the cylinder to leak out, eventually affecting the damper's performance. Additionally, the inability to evacuate the excessive heat from the coil trapped inside the fluid chamber and the complexity of carrying out maintenance in the case of a malfunction may compromise the efficiency of this solution.

As a result, a more viable solution is to install the magnetizing system around the existing hydraulic damper to create an external excitation system. The VFD can be designed with various sizes, configurations, and load capacities, depending on the application's specific requirements. The central VFD element for this research is a 2013 Mitsubishi L300 damper.

Fig. 5 shows an excitation system with coaxial coils placed externally around the VFD to generate the required magnetic field for the EC. The coils work together to generate a magnetic field in the axial direction. As the VFD rod moves up and down, the hollow electrode attached to the rod moves across the magnetic flux, inducing an EC that generates an additional electromagnetic damping force.

When designing an EC-based damping system, it is crucial to consider the system's specific requirements and choose the appropriate material based on factors such as cost, conductivity, and potential for corrosion. In addition to its dimensions, selecting the metallic tube material is critical for the system's proper functioning. The EC effect occurs when the magnetic field interacts dynamically with diamagnetic material. Aluminum and copper are both suitable for use in ECD systems as they are diamagnetic metals. Both materials have good corrosion
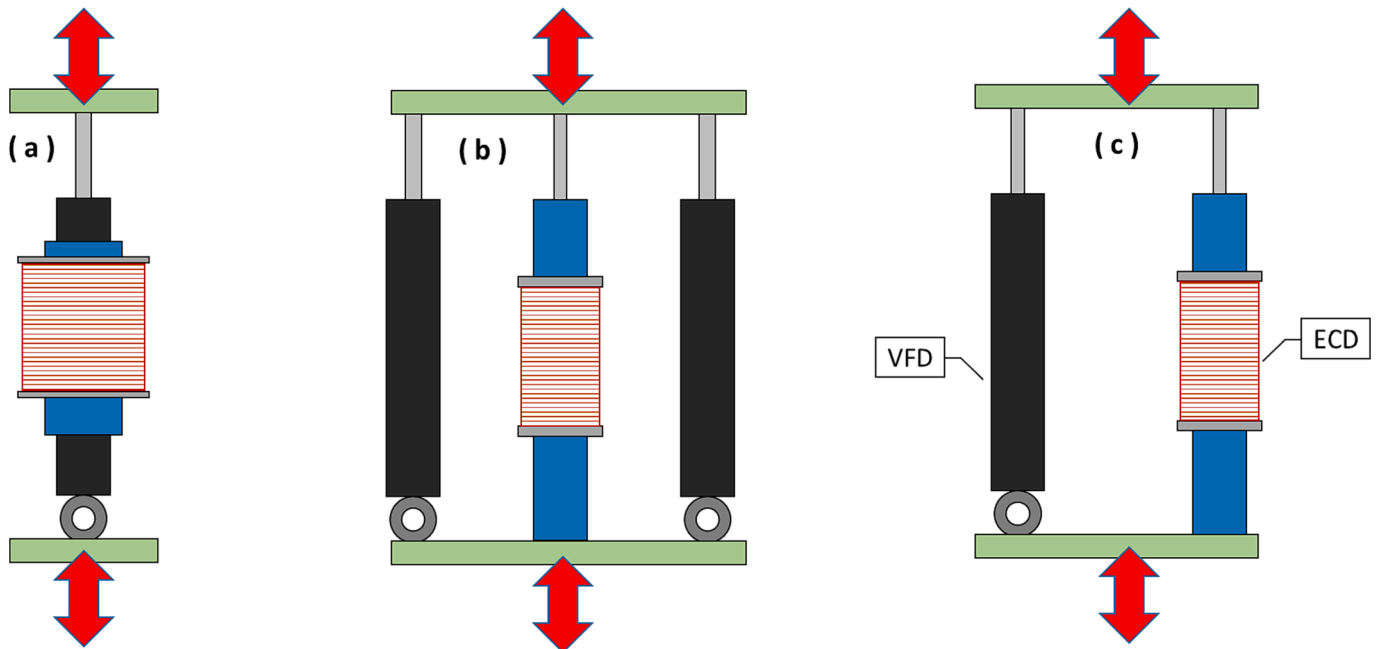

Fig. 3. Different configurations of combinations of the VFD and ECD. (a) coaxial parallel combination; (b) symmetric parallel combination; (c) asymmetric parallel combination.
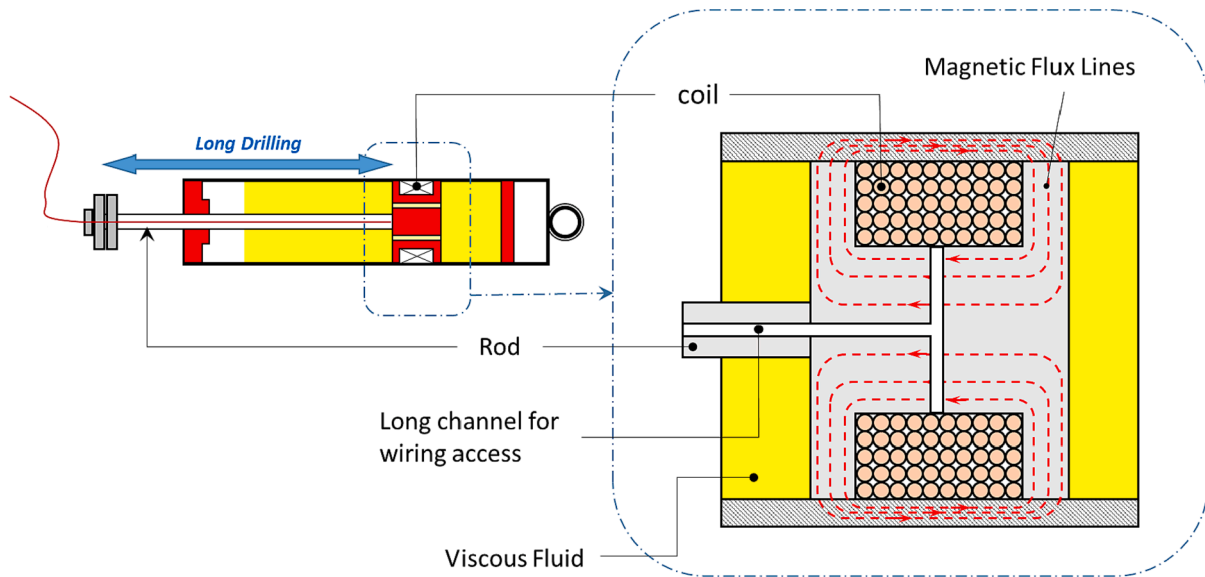
Fig. 4. Details of a combination of VFD and ECD with a magnetizing system inside the fluid chamber.
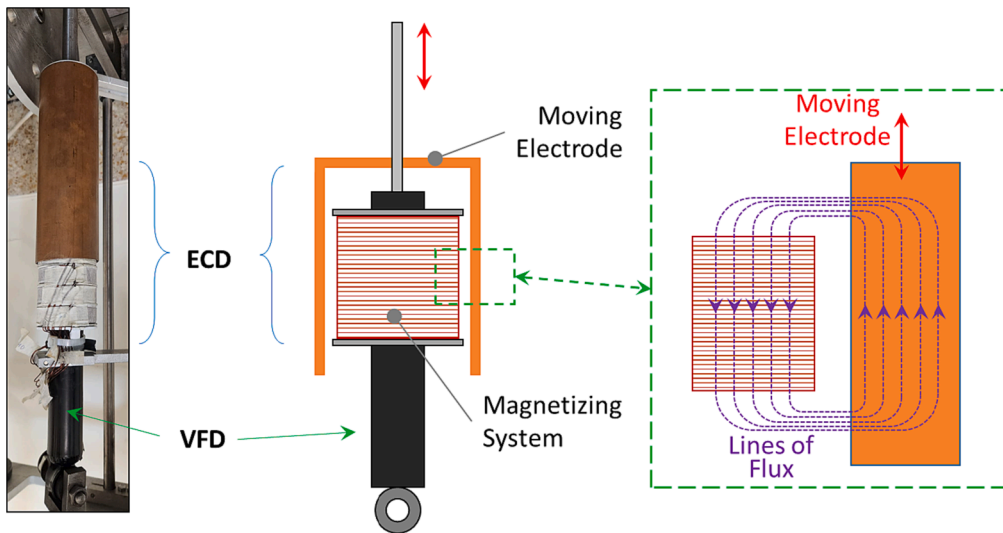

Fig. 5. The basic principle of the combined VFD and ECD.

resistance, which helps ensure the longevity of the damping system. Additionally, they are lightweight, making them ideal for reducing the overall weight of the damping system. However, some factors need to be taken into consideration. Copper is a better conductor of electricity than aluminum but is also more expensive. Moreover, copper has a higher thermal conductivity than aluminum, which can aid in dissipating heat generated by the ECD system.

Based on the previously mentioned constraints, a pipe made of copper was selected to be used as a moving electrode that will interact with an electromagnetic field created by a coil to generate the EC effect (Fig. 6).

3. Structural and magnetic analysis

3.1. Design of the magnetic excitation system

The magnetic field generated by a solenoid turns of wire all pass through the center of the coil and add (superpose) to produce a strong field there. The more turns of wire, the stronger the field produced. As

stated by Eq. (1), the magnetic flux density B is proportional to the the magnetic permeability constant μ_0, the number of turns N, and the current I circulating in the coil.

$$B = \mu_0 N I \tag{1}$$

Because of its shape, the field inside a solenoid can be very uniform and strong. However, the field just outside the coils is very weak because of the lines of flux dispersion (Fig. 7). Calculating the exact magnetic field at any point in space is mathematically complex and involves the study of Bessel functions.

The magnetic field flux lines must interact with the moving electrode to generate the EC effect. As per the "Lorentz force" equation (Eq (2), the interaction between the velocity and magnetic fields depends on the angular orientation between them,

$$\overrightarrow{F} = q\left(\overrightarrow{v} \times \overrightarrow{B}\right) \tag{2}$$

where q is the electric charge of the moving conductor.

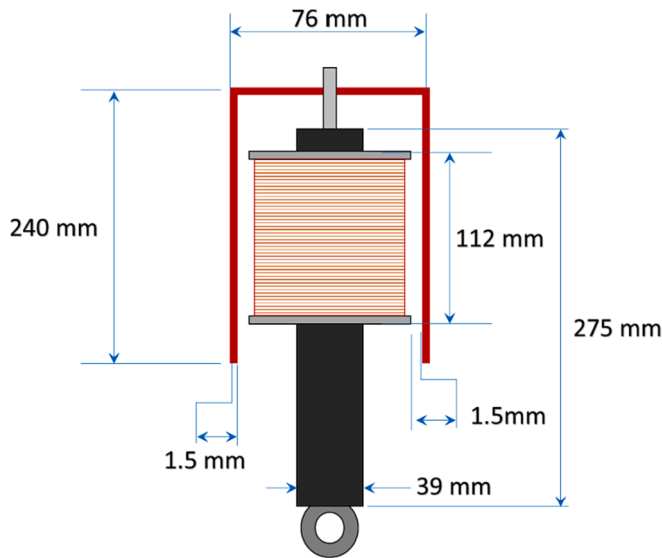As portrayed in Fig. 8, the force generated from the interaction

Fig. 6. Overall size and dimensions of the combined VFD–ECD system.

between the moving electrode and the magnetic field is maximum at the endpoints of the coil where the motion velocity is perpendicular to the magnetic field. However, the velocity is parallel to the magnetic field in the middle of the coil. Therefore, no interaction is observed there. Consequently, the EC effect will be perceived only at the endpoints of the solenoid.

As portrayed in Fig. 9, one method of increasing the interaction area and generating more EC effects consists of using two coaxial coils, insulated electrically from each other and having half of the turns in each.

From a magnetic point of view, and depending on the practical use, it is better to have one long coil than to divide it into two halves. This is because a long coil has more turns and produces a stronger magnetic field along its symmetry axis, more than two shorter coils. However, dual coils have different specifics depending on the orientation of the feeding currents. Indeed, from a magnetic point of view, if currents feed both coils in the same directions (Fig. 9a), the magnetic fields generated by each strand will cancel each other in their interface and yield virtually no external magnetic field. However, a new interaction zone is created at their interface when the two half coils are fed with current in opposite directions (Fig. 9b). With this newborn interaction zone, the EC effect will be more substantial. Moreover, the difference in electric resistance between one single coil and two halves of the same coil is that the dual coil combination will have half the resistance of the longer one

and produce less ohmic heating effects. The longer the wire, the more resistance there will be.

In summary, while a single coil generates a magnetic field of high intensity in its inner longitudinal direction and less affects the surrounding volume, a dual-coil configuration can obtain a more uniform magnetic field in the vicinity of the outer space surrounding the coil, where the interaction with the moving electrode is the most needed to generate the EC effect. Of course, the shorter the sub-coils, the greater the chances of interaction. However, the fragmentation process should not be carried too far to avoid having tiny, short coils with reduced electromagnetic effects. A good compromise should be reached in that case.

For practical considerations, five distinct coils with 180 turns each were considered a suitable replacement for one single coil with a total of 900 turns. For this research, AWG-22 coated copper wire with a diameter of 0.8 mm was used to produce the magnetic field in the ECD. While keeping the same overall number of turns, two different designs of coils were considered and numerically analyzed using COMSOL Multiphysics software. The first design consisted of one single solenoid with 900 turns (Fig. 10a), whereas for the second case, five solenoids with 180 turns each (Fig. 10b) were used, respectively. A 3D SolidWorks model was developed and then exported to COMSOL's magnetic field interface for each of these configurations.

To simulate the damping system, various domains were created using COMSOL software. These domains included the plastic holder, metallic core, magnetic coils, and an infinite spherical element to represent the air surrounding the excitation system (Fig. 11). The software's built-in physically controlled meshing was used to develop the mesh, which consisted of almost 104,553 tetrahedral elements and 20,486 triangular elements. The mesh's quality was deemed satisfactory as the average skewness was found to be 0.59, which is greater than the minimum value of 0.01 required, as reported in [27]. The materials for each domain were chosen from COMSOL's material library.

Two simulations were conducted with an excitation current of 2-A for each of the coils mentioned above, and contour plots of the resulting magnetic field are presented in Fig. 12. As previously expected, the fragmentation of the long coil into several short ones and feeding them with currents in opposite directions to generate magnetic polarities of the same type at the interfaces (such as N–S, S–N, N–S, S–N, N–S), focuses the magnetic field in the outer space at the vicinity of the coils, which is the region where the electrode will move and where the EC effect is expected to occur.

3.2. Design of the magnet holder

Designing a damper coil holder requires considering several aspects, such as the material, size, shape, and the environment in which it will be
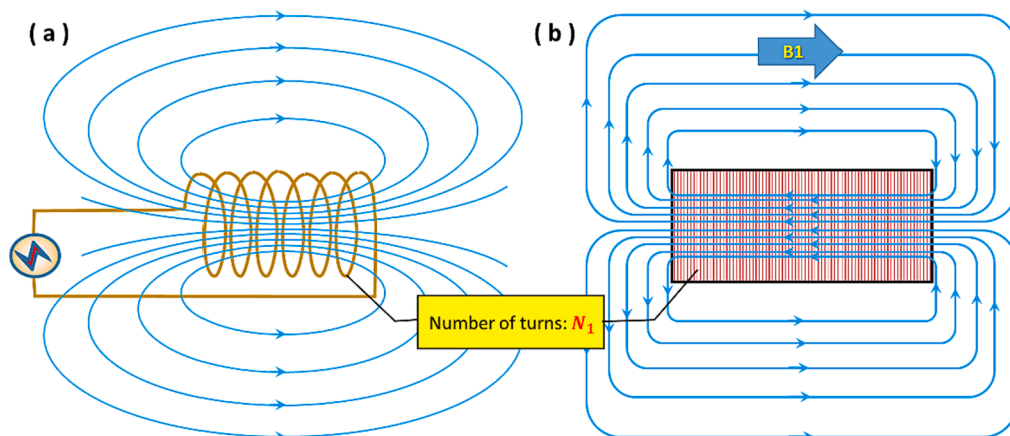

Fig. 7. Magnetic field and lines of flux generated by a single solenoid. (a) Realistic representation; (b) Symbolic representation.
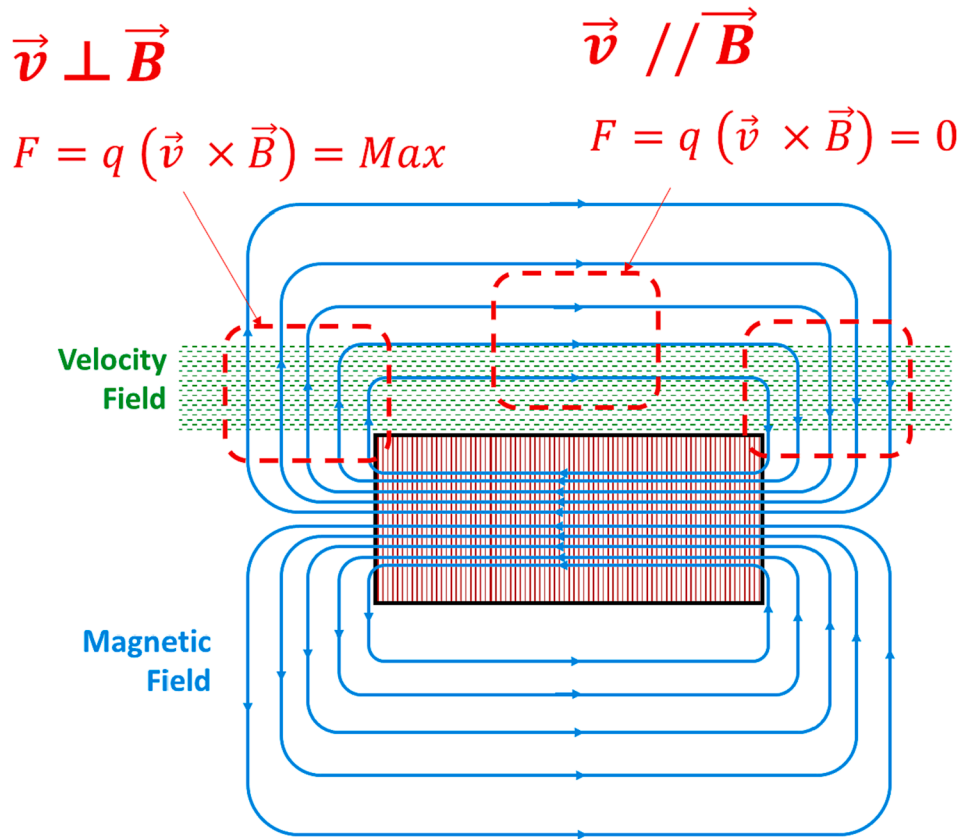
Fig. 8. Zones of interaction between magnetic and velocity fields.
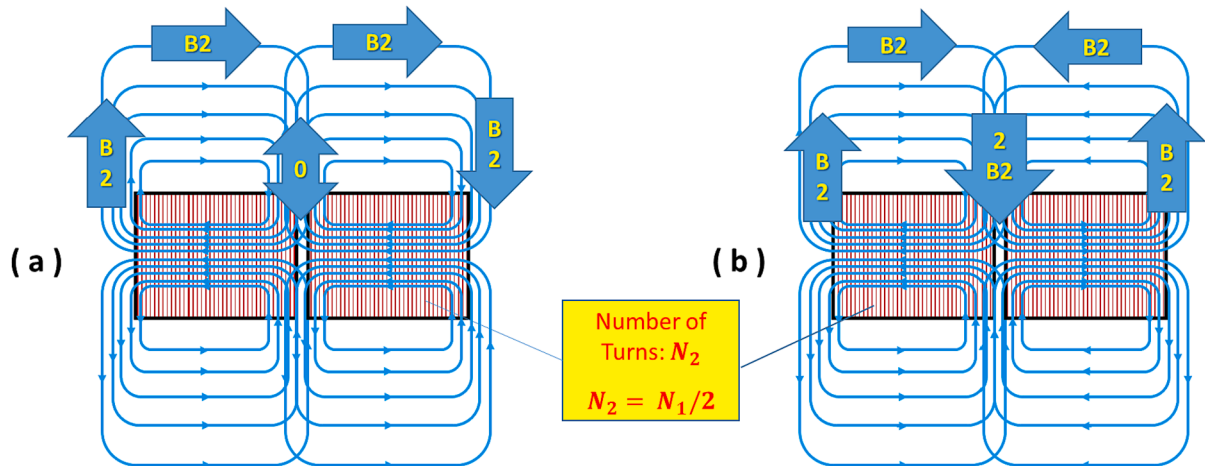

Fig. 9. Magnetic field obtained from the association of two halves of coils. (a) Feeding currents flowing in the same direction; (b) Feeding currents flowing in opposite directions.

used. Indeed, properly supporting the coil will extend its life and improve its working performance. The coil holder, commonly called the core, is a fundamental part of any magnetizing system. From a geometrical point of view, it should be designed to hold the coil securely in place while allowing for easy installation and removal if necessary, and it should also integrate seamlessly with the rest of the assembly. From a material point of view, the core should be metallic to increase the magnetic field produced by the coil. Adding a piece of ferromagnetic material, such as iron, in the center of the coil can considerably increase the magnetic field. Soft steel is often used as the core material for electro-magnets because it has a high magnetic permeability and low

residual magnetism. To accommodate five different coils, the core needs to be designed to facilitate easy and cost-effective manufacturing. Therefore, a set of six metallic rings, 2 mm thick, were welded equidistantly on a 55-mm mild steel pipe to form the core of the five solenoids. Finally, 180 turns of 0.8-mm AWG-22 coated wire copper were wound around each of the five sections of the metallic core to form five different electro-magnets.

The plastic core holder that fixes the set of coils to the damper's body was designed in two identical halves and 3D-printed (Fig. 13). To enhance the mutual bonding of the two parts and ensure good positioning between them, a tongue (bead) was made on one side and a
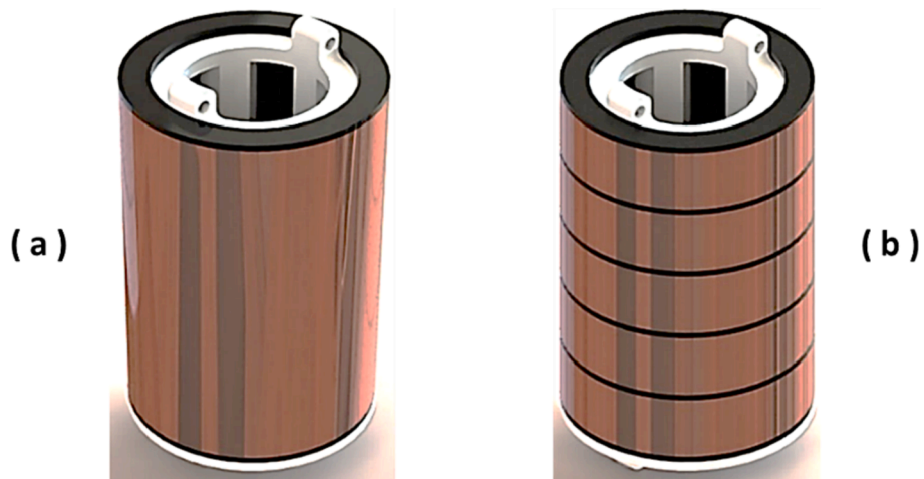
Fig. 10. Arrangement of the magnetic coils: (a) one solenoid with 900 turns; (b) five solenoids with 180 turns each.
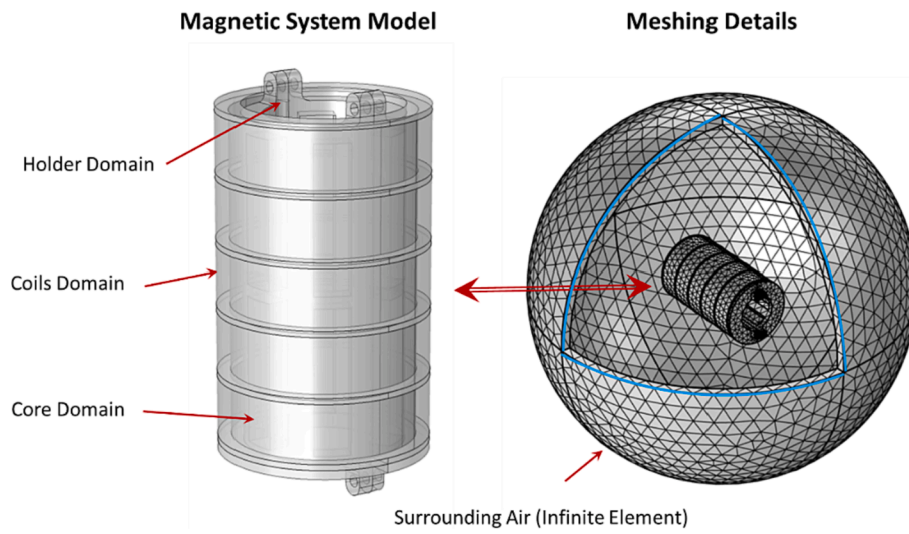

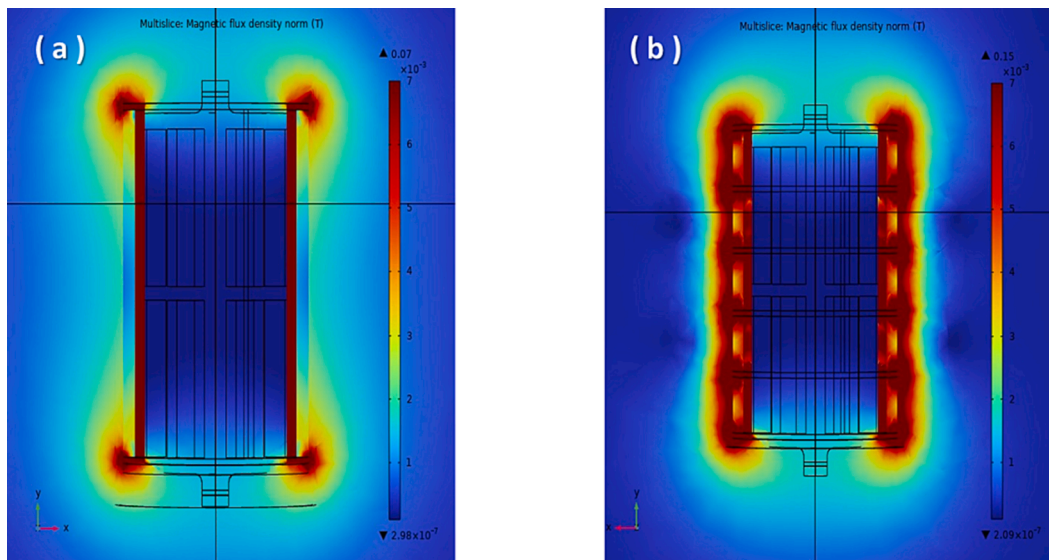**Fig. 11.** COMSOL model of a magnetic field.

Fig. 12. Contour plots of the magnetic field density: (a) single coil, (b) five coils.
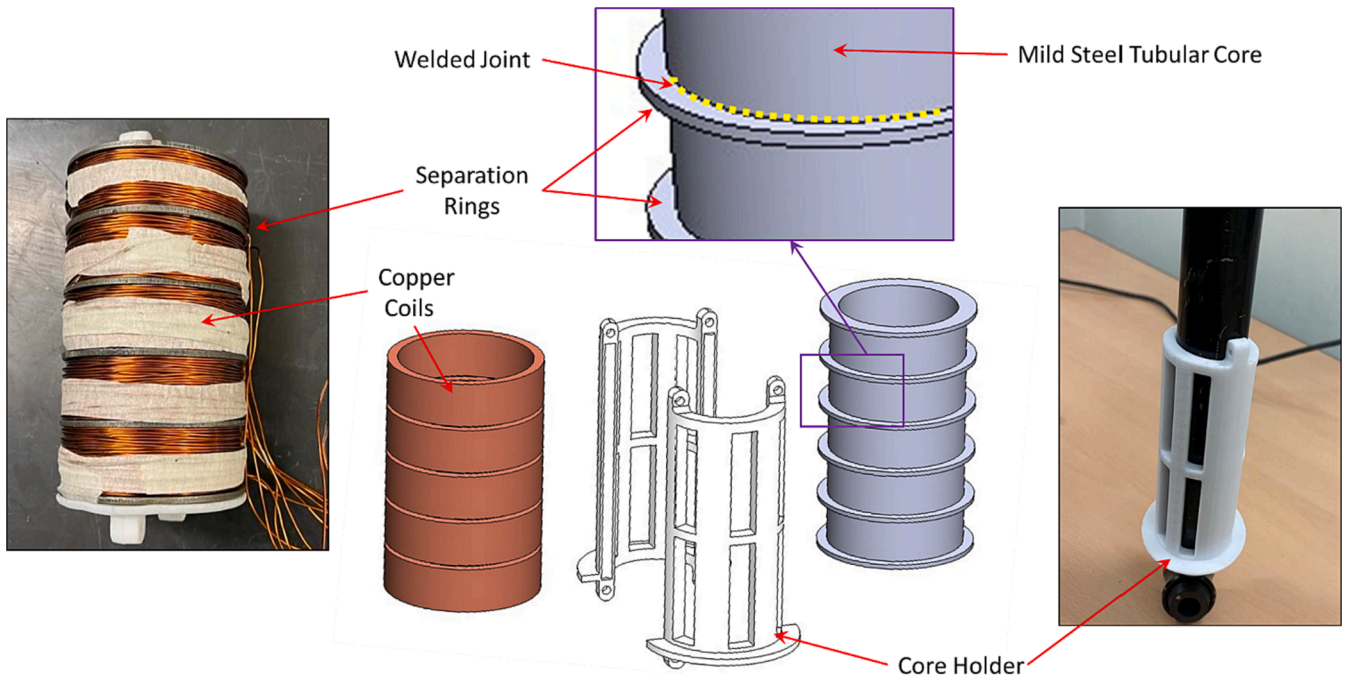
Fig. 13. Components of the magnetic field excitation system.

groove on the other. Mounting brackets were added to each part to allow bolts to join them together. Lateral openings were provided to allow enough ventilation of the coils. Restricting airflow will reduce their efficiency. Sharp edges were avoided everywhere; instead, rounded edges were used to prevent injury.

4. Experimental setup of the ECD

A custom-made testing rig was designed and developed to validate the efficiency of the proposed ECD. The testing setup (Fig. 14) consisted of two thick parallel plates with four long neck flanges at each corner to make a stable frame that would not affect the readings' accuracy. Moreover, a sliding mechanism composed of a Scotch yoke plate supported by two linear bearings was used to transform the continuous rotational motion of the disk into the damper's linear sinusoidal motion.

As portrayed in Fig. 15, two different sensors were mounted on the system to read the experimental data and quantify the efficiency of the ECD damper. First, a linear variable differential transducer (LVDT) (from Loadstar, model number LVDT-100 M−A) with a 100-mm reading range was installed between the top of the damper's body and the low end of the conductor pipe. This LVDT sensor recorded the damper's linear displacement (with an overall error of 0.02 % on a full scale). The
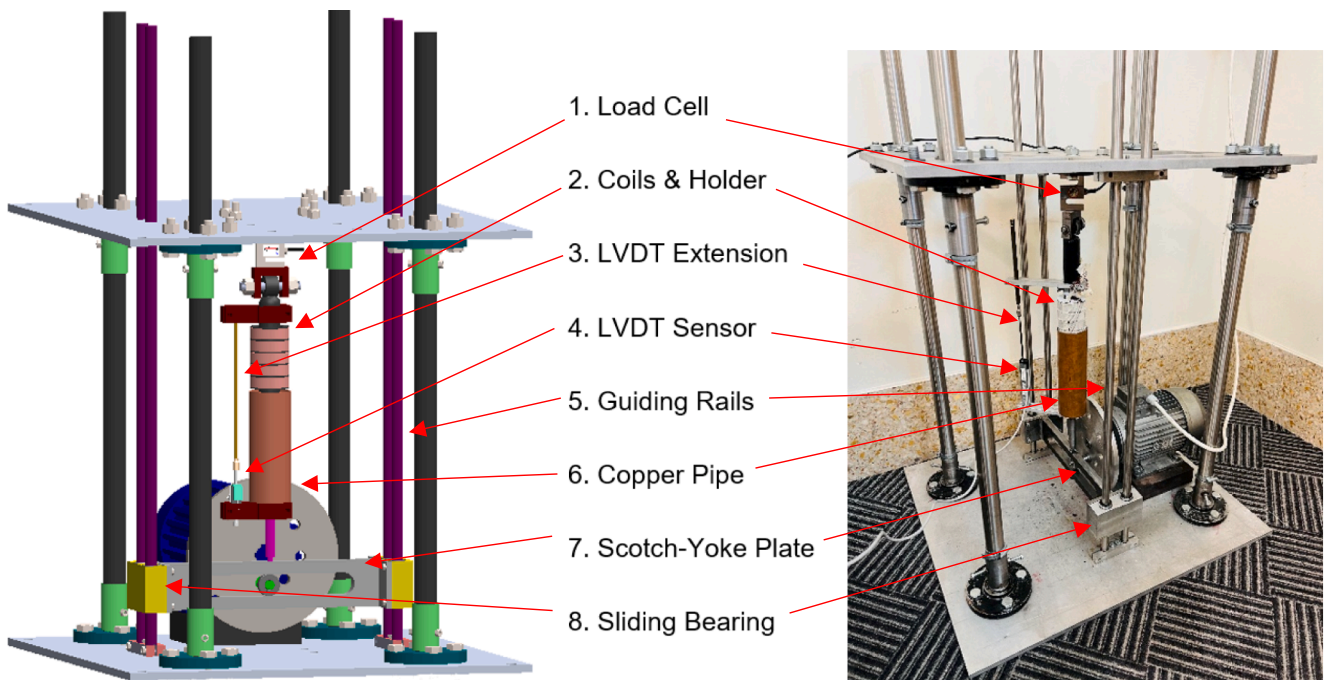

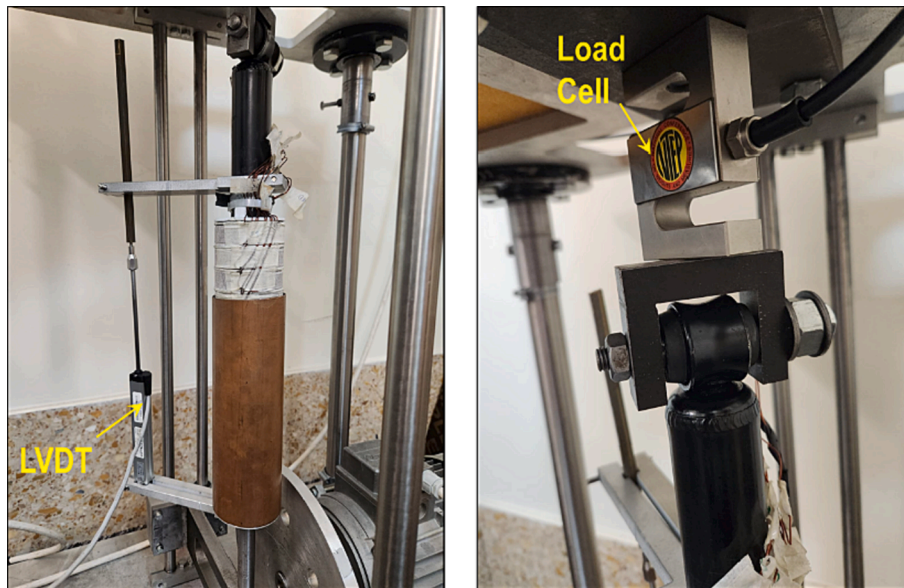**Fig. 14.** Experimental setup of the ECD.

Fig. 15. Different types of sensors mounted on the test rig.

second sensor was an S-Beam Load Cell Sensor (from Loadstar, model number RAS1-500S-S) with an overall error of 0.02 % on the full scale. It was fixed in series between the uppermost part of the frame and the top of the damper's body to measure any changes in the damping force among the testing intervals. Finally, a variable frequency controller (VFC) from Schneider (model number 3 kW-ATV312HU30N4) was connected to a three-phase 1.87 kW VEMAT motor to maintain a fixed rotational speed of 25 rpm during all tests. The tests were carried out while the ECD was supplied with a current varying from 0 to 5 A. Several readings were taken for each case at the same speed to ensure validity and repeatability.

5. Results and discussion

Once the test rig had been completely mounted and tuned, two experiments were conducted on the combined VFD–ECD device without and with an excitation current. Each test subjected the damper to a periodic load from the sliding motor setup, in which the speed was kept at a constant value. Meanwhile, the electric current applied to the coils was increased from 0 to 5 A at a step of 1 A, but the value remained

constant during each experiment. Fig. 16 portrays examples of the experimental results obtained from the displacement sensor (LVDT) readings for the case of an excitation current of 0 A and 1 A.

A Scotch yoke (sometimes called a slotted link mechanism) is a mechanism with a reciprocating motion designed to convert a disc's rotational motion into the linear motion of a slider and vice versa. Compared with other mechanisms using reciprocating motion, the Scotch yoke mechanism has several advantages, such as the reversibility of the motion, easy assembly and operation, and smoother operation due to fewer moving components. However, it also has several disadvantages, including the need for precision machining, high wear and tear on the sliding components, and the potential for high-impact forces. Moreover, because the lever had a greater length at the ends of the stroke, a certain level of force produced more torque at the extreme points of the path of motion than in the middle. Because of its construction, the Scotch yoke mechanism has a controlled displacement with a fixed amplitude. In the actual configuration, the translating pin was set to have a radius of 50 mm, limiting the peak-to-peak amplitudes for both displacement graphs (Fig. 16) to 100 mm.

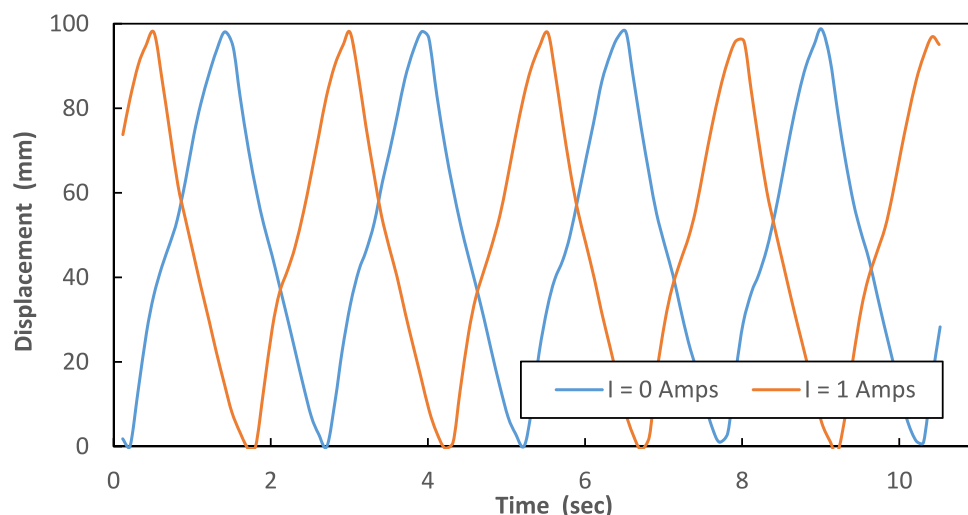Even though the peak-to-peak amplitudes remained constant, an

Fig. 16. Experimental results of the LVDT readings: Displacement vs. time for I = 0 A and I = 1 A.

analysis of the variation in the shape revealed that an increase in current excitation intensity is found to create a time delay in the response of the driven mechanism. By applying a numerical derivative twice, the acceleration of the moving mechanism was computed and displayed in Fig. 17.

One can see that after feeding the coils with an excitation current, the EC phenomenon produced by the interaction of the moving copper electrode and the magnetic field generated more drag effects that slowed down the motion of the moving parts and reduced its acceleration. The previous curves showed a decrease in the acceleration's peak amplitude from around 3.0 m/s² to 2.45 m/s², i.e., a reduction of about 18 % in the peak value. This preliminary result practically confirmed the effectiveness of the ECD when added to the VFD for reducing the disturbance transmitted through the damping device. However, as portrayed in Fig. 18, any further increase in the current was insignificant as the limit of acceleration limit was reached. This is the magnetic saturation phenomenon discussed earlier in the introduction. When an increase in the external magnetic field does not increase the material's magnetization beyond a specific value, the total magnetic flux density levels off, a state known as magnetic saturation.

To better understand the EC effect, the results obtained from the force sensor for the cases with an excitation current of 0 A and 1 A are displayed in Fig. 19.

A glance at the force–time graphs in Fig. 19 shows the nonharmonic behavior of the force sensor readings. The distortion observed in this graph is most probably due to two phenomena: the damper's internal functioning and the way it was driven. Indeed, the Scotch yoke mechanism used in this test rig was theoretically supposed to convert the constant-speed rotational motion of the disc into the pure harmonic oscillatory linear motion of the damper. However, because of the non-negligible weight of the moving mechanism (the Scotch yoke and two linear bearings), the cycle's limits are always accompanied by extra shocks that distort the shape of the force graph's waves. The internal malfunction will be discussed later.

Despite this unusual finding, one can see that the amplitude of maximum force increased with an increase in the current feeding the solenoids. When the current increased from 0 to 1 A, the driving system required approximately 12 % more force (from 180 N to 202 N) to move the VFD rod over the same distance (100 mm). This result confirmed the ability of the ECD to have a noticeable effect on the original VFD.

Driving the damper by the prescribed displacement waveform displayed in Fig. 16 results in a force–velocity loop represented in Fig. 20. Several cycles of loading/unloading curves are plotted. From a first look, one can see that the curves are not symmetrical, shifted upward from the origin, and not superposing with each other.

The fundamental velocity-dependent nature of damping combined with physical nonlinearities introduce asymmetry into the force–velocity curve, making it not symmetric, with different damping behavior for the compression (bump) and extension (rebound) cycles. This asymmetrical relationship can be attributed to several factors. First, it is crucial to acknowledge that automotive dampers are designed to counteract dynamic loads and dissipate energy only at the rebound. Indeed, contrary to what is commonly understood, when the vehicle rolls over a bump, the spring absorbs the initial compressive excitation. This fact naturally breaks the symmetry of the device. However, in our case, the asymmetry is amplified by various internal parameters, such as manufacturing imperfection. Moreover, contrary to most cases, the force–velocity curve is not centered around the origin, which pinpoints an internal problem inside the damper.

Hysteresis in the force–velocity graph of a damper refers to the phenomenon where the damping force experienced for a given velocity depends on the direction of motion. To recognize hysteresis in the force–velocity graph of a damper, one needs to look for a loop in the graph. When the damper is compressed (negative velocity), the damping force follows one curve. However, when the damper extends (positive velocity), the damping force follows a different curve for the same velocity magnitude. This creates a loop or hysteresis in the force–velocity graph instead of a single curve. Hysteresis is unavoidable, but it can be kept to a minimum by pressure tuning. Contrary to most cases where a distinctive S-shaped curve is observed, the actual curves shown in Fig. 20 show a totally different shape. Such a discrepancy is probably due to poor manufacturing quality.

A closer look at the force–velocity graph for one loading cycle is displayed in Fig. 21. One can see that the damping force increases linearly at low damper velocity. The same linear behavior is observed when the VFD is combined with an ECD. In that case, if the excitation current is 1A, there is a 22 % increase in the slope.

Finally, the maximum force amplitude was measured for different magnetic excitation currents, ranging from 0 to 5 A, with a step of 1 A. In order to reduce the experimental error and ascertain the results' accuracy, the experiment was repeated three times each for all six excitation currents. The average value of the force amplitude was then computed for the three trials and plotted against the excitation current, as shown in Fig. 22.

The EC effect was quickly noticed in the presence of electric excitation of the magnetizing system, and a sudden jump was clearly recorded. However, any further increase in the current did not push that limit further. Because of magnetic saturation, the maximum damping
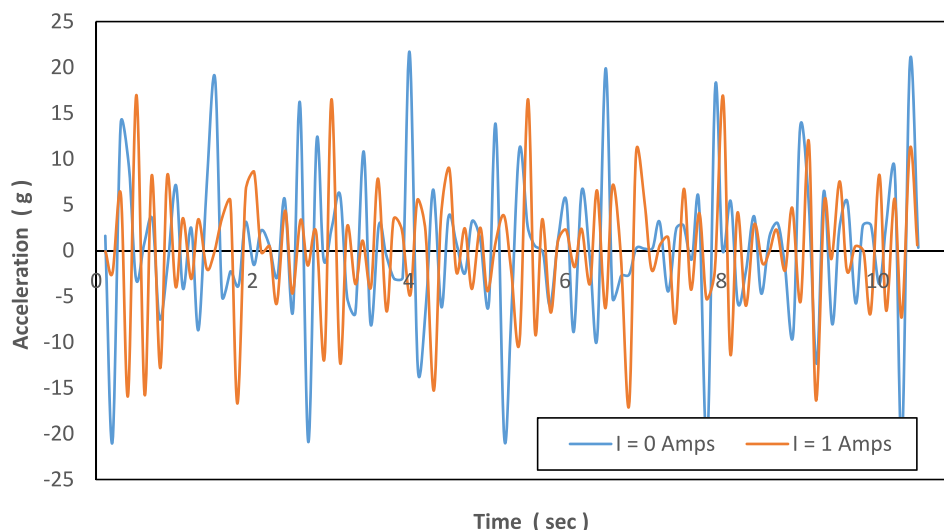

Fig. 17. Double derivatives of the experimental LVDT readings: Acceleration vs. time for I = 0 A and I = 1 A.
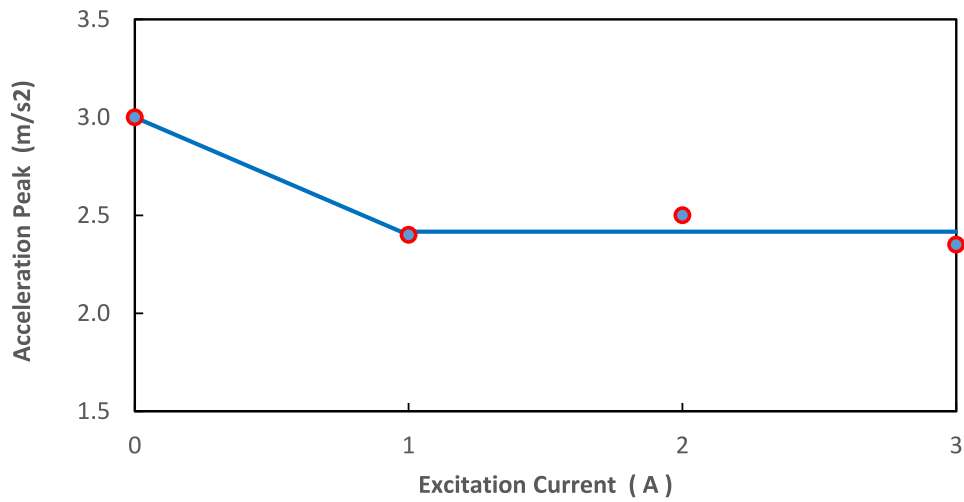
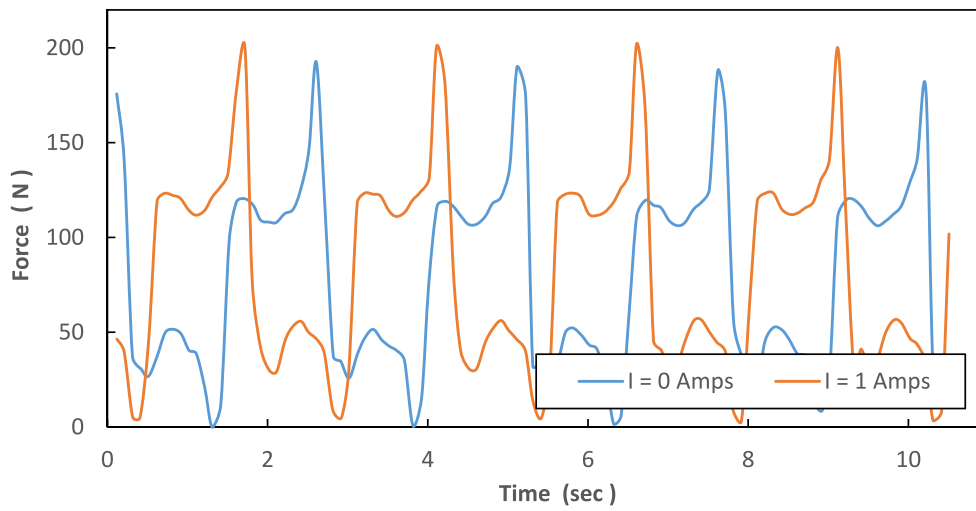**Fig. 18.** Effect of magnetic saturation on the peak acceleration of the experimental LVDT readings.

Fig. 19. Experimental results of the force sensor readings: Force vs. time for I = 0 A and I = 1A.
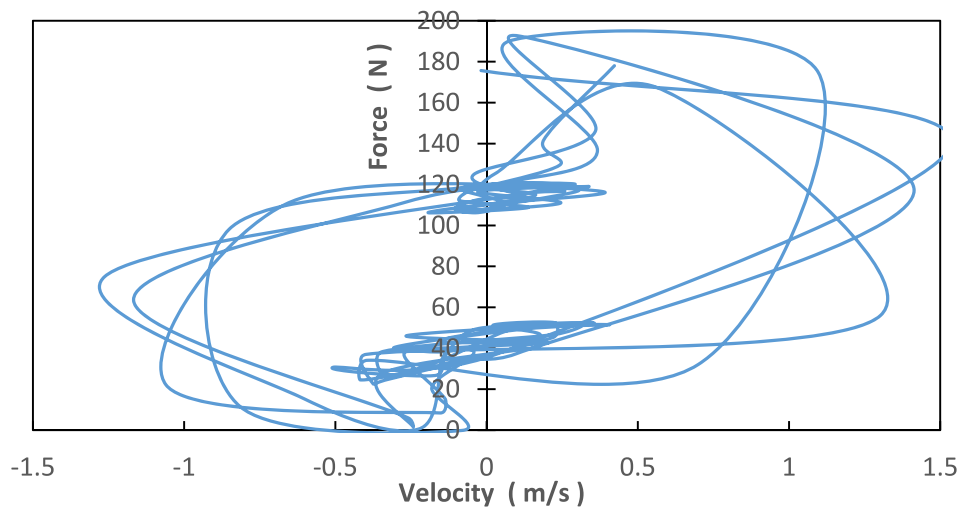
Fig. 20. Force-Velocity graph for the viscous-fluid damper without EC effect.
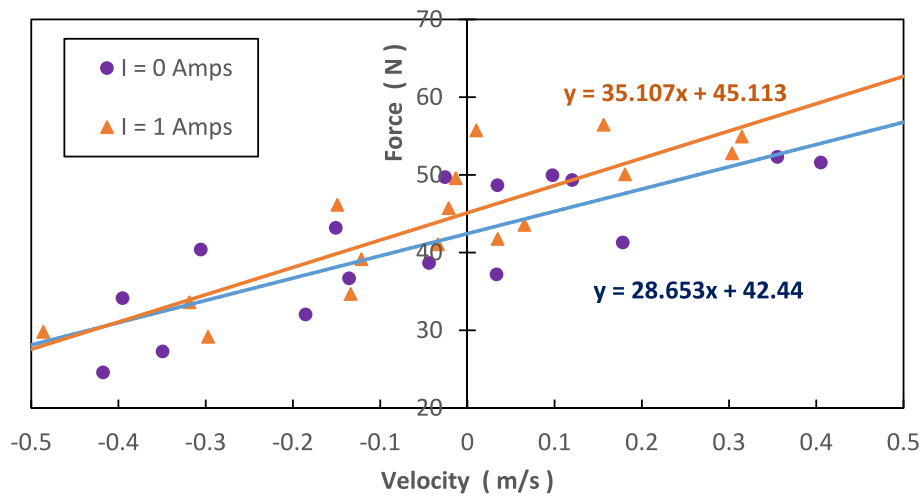
Fig. 21. Force-Velocity graph for the VFD-ECD combination, for I = 0 A and I = 1 A.
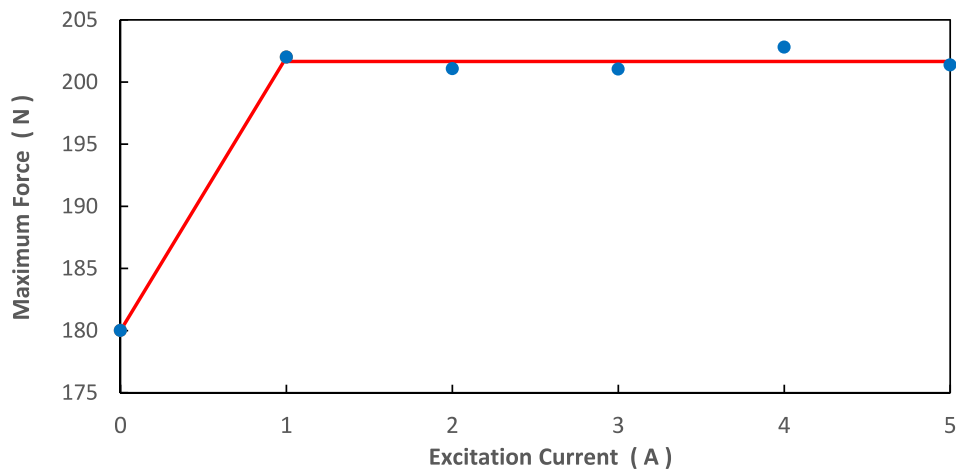

Fig. 22. Amplitude of the driving forces vs. excitation current.

force of 202 N remained nearly identical for the different excitation currents.

Increasing the thickness of the moving copper electrode is generally beneficial for overcoming magnetic saturation. However, other factors,

such as the material type and the magnetic excitation amplitude, can also affect magnetic saturation. To quantify these effects, the time a magnet took to slide along an inclined plate (the sliding time) of aluminum and copper was recorded in our lab. The results are

Table 1
Time taken to slide over inclined plates of different materials and thicknesses.

Material	Thickness (mm)	Trial 1 time (s)	Trial 2 time (s)	Average time (s)	
Copper	1	2.63	2.53	2.58	
Aluminum	1	1.62	1.66	1.64	
Aluminum	3	2.85	2.70	2.77	

summarized in Table 1.

As a result of the previous elementary experiment, one can conclude that a threefold increase in the thickness increased the sliding time by 69 %. Contrary to what was expected beforehand, the relationship between the conductor's thickness and the EC effect was nonlinear. This behavior mainly occurred because the ECs were concentrated close to the surface nearest to an excitation coil, and their strength decreased exponentially with depth, which is called the skin effect. Indeed, the depth to which the ECs can penetrate a material is influenced by the excitation current's frequency and the specimen's magnetic permeability and electrical conductivity. The penetration depth decreased with conductivity, frequency, and magnetic permeability increase. Therefore, increasing the thickness of a metal conductor can increase its saturation level, but there is a limit to the amount of magnetic field that can be induced in a material, so increasing the thickness beyond that limit will not result in any additional magnetic induction.

6. Conclusions

In conclusion, enhancing the efficiency of a shock absorber and increasing its ability to absorb shocks by relying on the EC principle was proved in this study. A manufactured ECD magnetic excitation system surrounded a commercial viscous damper and was then experimentally tested to examine its efficiency. Firstly, three different designs for the magnetic circuit were proposed and modeled numerically using COMSOL's magnetic field interface. The numerical investigation revealed that five sets of coils were better than one set of coils in terms of the magnetic field's density. The selected excitation system was manufactured and assembled with a VFD to develop the desired ECD. The ECD's behavior was investigated experimentally using a reciprocating motor with a sliding bearing. The test was made at a fixed speed while the magnetic excitation current was increased in steps of 1 A from 0 A to 5 A. The test investigated the contribution of the magnetic drag force and its effects on the ECD's damping effect. Besides the disturbance introduced by the damper's quality and the test rig's imperfections, the results confirmed the dependence of the damping force on the excitation current feeding the magnetizing system.

Furthermore, at 1 A, the damping force increased by 12 % compared with the case without excitation. However, the forces stayed almost the same over the rest of the excitation currents. The EC system reached magnetic saturation, which prohibited any further increase in the damping forces. Increasing the thickness of the copper tube may be a simple way to overcome this limitation practically.

7. Declaration of generative AI in scientific writing

The author(s) reviewed and edited the content as needed and took full responsibility for the publication's content.

Declaration of competing interest

The authors declare that they have no known competing financial interests or personal relationships that could have appeared to influence the work reported in this paper.

Data availability

Data will be made available on request.

Acknowledgments

References

[1] Movotiv, 2023. On global journeys and Markets (mostly pre-Covid). Available at https://movotiv.com/statistics (accessed 2 June 2023).

[2] S. Ishii, Y. Sakai, R. Suka, Y. Aoki, M. Asanuma, Development and evaluation of electro rheological fluid utilizing ion conductive polyurethane particles for semi-active suspension, Trans. Soc. Automot. Eng. Jpn. 53 (2022) 233–239.

[3] S. Sassi, K. Cherif, Combination of homogeneous electro-rheological fluid and multi-electrodes damper for a better control of car suspension motion, Int. J. Mech. Sys. Eng. 2 (2016) 112, https://doi.org/10.15344/2455-7412/2016/112.

[4] Y. Badri, T. Syam, S. Sassi, M. Hussein, J. Renno, S. Ghani, Investigating the characteristics of a magneto-rheological fluid damper through CFD modeling, Mater. Res. Express 8 (2021), 055701, https://doi.org/10.1088/2053-1591/abfcf6.

[5] M.H. Idris, F. Imaduddin, M. Ubaidillah, S.A. Mazlan, S.B. Choi, A concentric design of a bypass magneto-rheological fluid damper with a serpentine flux valve, Actuators 9 (2020) 16, https://doi.org/10.3390/act9010016.

[6] Y. Badri, A. Alhams, S. Sassi, M. Hussein, J. Renno, Enhancing the Damping Effect of MRF Damper Using an External Magnetic Excitation System, Mater. Res. Express 10 (2023), 095703, https://doi.org/10.1088/2053-1591/acfae5.

[7] T. Szmidt, D. Pisarski, R. Konowrocki, Semi-active stabilisation of a pipe conveying fluid using eddy-current dampers: state-feedback control design, experimental validation, Meccanica 54 (2019) 761–777, https://doi.org/10.1007/s11012-019-00988-3.

[8] B. Ebrahimi, M.B. Khamesee, F. Golnaraghi, Eddy current damper feasibility in automobile suspension: modeling, simulation and testing, Smart Mater. Struct. 18 (2009), 015017, https://doi.org/10.1088/0964-1726/18/1/015017.

[9] L. Zuo, X. Chen, S. Nayfeh, Design and analysis of a new type of electromagnetic damper with increased energy density, J. Vibr. Acoust., Trans. of the ASME 133 (2011), 041006, https://doi.org/10.1115/1.4003407.

[10] J. Theunissen, A. Tota, P. Gruber, M. Dhaens, A. Sorniotti, Preview-based techniques for vehicle suspension control: a state-of-the-art review, Annu. Rev. Control. 51 (2021) 206–235, https://doi.org/10.1016/j.arcontrol.2021.03.010.

[11] H.Y. Zhang, Z.Q. Chen, X.G. Hua, Z.W. Huang, H.W. Niu, Design and dynamic characterization of a large-scale eddy current damper with enhanced performance for vibration control, Mech. Syst. Sig. Process. 145 (2020), 106879, https://doi.org/10.1016/j.ymssp.2020.106879.

[12] Z. Lu, Z.Q. Huang, X. Lu, Experimental and analytical study on vibration control effects of eddy-current tuned mass dampers under seismic excitations, J. Sound Vib. 421 (2018) 153–165.

[13] B. Ebrahimi, M.B. Khamesee, F. Golnaraghi, Permanent magnet configuration in design of an eddy current damper, Microsyst. Technol. 16 (2010) 19–24, https://doi.org/10.1007/s00542-008-0731-z.

[14] W. Chen, J. Jiang, J. Liu, S. Bai, W. Chen, A passive eddy current damper for vibration suppression of a force sensor, J. Phys. D. Appl. Phys. 46 (2013), 075001, https://doi.org/10.1088/0022-3727/46/7/075001.

[15] Yi, Z., Hong, Z., Hui-Zhi, S., 2010. Research of the orthoscopic permanent magnet eddy current damper in magnetic stage. In 2010 International Conference on Computer Application and System Modeling (ICCASM 2010). IEEE (pp. V14-354–V14-356). https://doi.org/10.1109/ICCASM.2010.5622271.

[16] Z. Wang, Z. Chen, J. Wang, Feasibility study of a large-scale tuned mass damper with eddy current damping mechanism, Earthquake Eng. and Eng. Dyn. 11 (2012) 391–401, https://doi.org/10.1007/s11803-012-0129-x.

[17] W. Yu, G. Yang, Eddy current damper capable of collecting electric energy, Vibroeng. Procedia 33 (2020) 28–33, https://doi.org/10.21595/vp.2020.21672.

[18] Y. Takayama, S. Kijimoto, S. Ishikawa, Eddy current damper model of ring magnet and coaxially moving conducting disk, IEEE Trans. Magn. 57 (2021) 1–13, https://doi.org/10.1109/TMAG.2021.3058739.

[19] P. Bong-Do, K. Jong-Hyuk, B. Jae-Sung, A study on vibration attenuation of structure applied on eddy current damper, Int. J. Aeronaut. Space Sci. 23 (2022) 906–915, https://doi.org/10.1007/s42405-022-00495-y.

[20] U. Jamolov, G. Maizza, Integral methodology for the multiphysics design of an automotive eddy current damper, Energies (basel) 15 (2022) 1147, https://doi.org/10.3390/en15031147.

[21] A.I.A. Eisa, L. Shusen, Z. Yan, W.M.K. Helal, Transient analysis method of an axially magnetized novel passive eddy current damper for suppressing lateral vibrations, Math. Probl. Eng. 2022 (2022) 3808992, https://doi.org/10.1155/2022/3808992.

[22] C. Zhang, N. Sang, S. Qiu, S. Chen, R. Li, M. Yang, G. Yang, A dual-sided hybrid excitation eddy current damper with high-conductivity and high-permeability secondary plate for vibration suppression enhancement, J. Vib. Eng. Technol. 11 (2022) 1229–1240, https://doi.org/10.1007/s42417-022-00638-1.

[23] U. Jamolov, F. Peccini, G. Maizza, Multiphysics design of an automotive regenerative eddy current damper, Energies (basel) 15 (2022) 5044, https://doi.org/10.3390/en15145044.

[24] M. Putra, M. Nizam, D. Tjahjana, H. Waloyo, The effect of air gap on braking performance of eddy current brakes on electric vehicle braking system, in: Sixth International Conference on Electric Vehicular Technology (ICEVT), IEEE, Bali, Indonesia, 2019, pp. 355–358, https://doi.org/10.1109/ICEVT48285.2019.8993987.

[25] Z.-G. Zhi-Gao Li, Y. Yang, A.-Z. Liu, Z.-D. Jia, D.-X. Huang, L. Liu, N. Yan, Y.H. Ding, J.-J. Sun, Z.-H. Zhang, S.-K. Ren, Energy storage in magnetic devices air

gap and application analysis, Energy Rep. 8 (2022) 152–161, https://doi.org/10.1016/j.egyr.2022.09.124.

[26] Z. Zeng, P. Ding, J. Li, S. Jiao, J. Lin, Y. Dai, Characteristics of eddy current attenuation and thickness measurement of metallic plate, Chin. J. of Mech. Eng. 32 (1) (2019) 1–9, https://doi.org/10.1186/s10033-019-0419-6.

[27] J. Gothäll, How to Inspect Your Mesh in COMSOL Multiphysics®, COMSOL Multiphysics. (2022).